Applied Thermal Engineering 188 (2021) 116557

Contents lists available at ScienceDirect

Applied Thermal Engineering

journal homepage: www.elsevier.com/locate/apthermeng

Analysis and prediction of the performance of free- piston Stirling engine using response surface methodology and artificial neural network

Wenlian Ye [a,*], Xiaojun Wang [b], Yingwen Liu [c], Jun Chen [a]

[a] College of Mechanical and Electronic Engineering, Northwest A&F University, Yangling, Shaanxi 712100, PR China
[b] Key Laboratory of Vacuum Technology and Physics, Lanzhou Institute of Physics, Lanzhou, Gansu 730000, PR China
[c] Key Laboratory of Thermo-Fluid Science and Engineering of MOE, School of Energy and Power Engineering, Xi'an Jiaotong University, Xi'an, Shaanxi 710049, PR China

ARTICLE INFO

Keywords:
Free-piston Stirling engine
Response surface methodology
Artificial neural network
Performance prediction

ABSTRACT

Free piston Stirling engine is a popular area of research in high-efficiency thermal power conversion technology. However, owing to its strong coupling, nonlinearity, and parameter interactions, building an effective model to predict the performance is of great importance. This study was to investigate and derive the prediction models of a nonlinear free-piston Stirling engine using response surface methodology and artificial neural network. The interactive influences of thermodynamic and dynamic parameters which have significant effects on the amplitudes of the displacer and piston, operating frequency, and output power were illustrated in detail. Also, error analyses were then performed between the simulated and predicted values for both methods by comparing the mean absolute percentage errors, mean-squared errors, and correlation coefficients. The results indicated the correlation coefficients for the four output parameters from the response surface methodology as 0.9998, 0.9998, 0.9999, and 0.9994, and approximately 95% of the output parameter data were predicted with $< 5\%$ errors during verification, indicating that the response surface methodology model had good predictability compared with the artificial neural network model. Therefore, this research provides an effective approach to predict performances and can be applied to optimise the Stirling engine performance accurately and quickly.

1. Introduction

Free piston Stirling engines (FPSEs) can utilise several kinds of heat sources, such as radioactive isotope heat sources, solar energy, biomass, and nuclear energy [1-3], to convert thermal energy into mechanical energy, which is a popular area of research in high-efficiency thermal power conversion technology in recent years [4,5]. An FPSE is a variable form of Stirling engine that does not require the crank shaft compared to a traditional kinematic Stirling engine [6]; this type of engine has advantages such as high efficiency, high reliability, long life, low pollution, and simple structure. The movements of the displacer and piston are induced by gas pressure variations within this engine; thus, two pistons can move independently of each other, and the operating frequency can be determined by the spring- mass-damper of the system, indicating that the FPSE is a multi-degree-of-freedom system [7]. The various configurations of FPSEs can be generally classified into alpha, beta, and gamma types. The gamma-type FPSE is the primary focus of this research.

Although the FPSE has many advantages, its performance prediction and dynamic analysis are challenging for designers. As noted above, the movements of the displacer and piston are determined by various thermodynamic and dynamic parameters. Owing to the interrelated thermodynamic–dynamic parameters, strong coupling between the FPSE's thermodynamic and dynamic characteristics is obtained, rendering complicated dynamic behaviors.

The Schmidt isothermal model has been adopted in most dynamic analyses of FPSEs [8–10]. A summary of prior study on the analyses of the FPSE has been listed in Appendix A. There has been a lot of studies done on the FPSE performance analyses both experimentally and theoretically, and the conclusions show that the thermodynamic and dynamic parameters have significant impacts on the stability of the linear and nonlinear FPSE system. Most results from theoretical research indicate that the FPSE system can operate stably with a range of operating and dynamic parameters, such as the hot-end temperature, cold-end temperature, charge pressure, piston's damping, and the stiffness of the pistons [8–11,14]. A mathematical form for operating frequency, phase angle, and pistons amplitude ratio was derived in the linear FPSE

* Corresponding author at: College of Mechanical and Electronic Engineering, Northwest A & F University, Yangling, Shaanxi 712100, PR China.
E-mail address: ywl-315@nwafu.edu.cn (W. Ye).

https://doi.org/10.1016/j.applthermaleng.2021.116557
Received 30 September 2020; Received in revised form 25 December 2020; Accepted 2 January 2021
Available online 30 January 2021

Nomenclature

A	cross-sectional area, m^2
c_d	displacer damping coefficient, $V{\cdot}s{\cdot}m^{-1}$
c_{dd}	viscous damping of the displacer, $V{\cdot}s{\cdot}m^{-1}$
c_p	piston damping coefficient, $V{\cdot}s{\cdot}m^{-1}$
c_{pp}	viscous damping of the piston, $V{\cdot}s{\cdot}m^{-1}$
D	damping coefficient, m^{-1}
[D]	matrix of damping coefficients
f	frequency, Hz
F_{load}	external load force which is attached to the piston, N
k_{alt}	load damping coefficient, $V{\cdot}s{\cdot}m^{-1}$
k_c	nonlinear coefficient of the load, $N{\cdot}s{\cdot}m^{-3}$
K	stiffness coefficient per mass unit, $N{\cdot}m^{-1}{\cdot}kg^{-1}$
[K]	matrix of stiffness coefficients
m	mass, kg
[M]	matrix form of differential equations
p	pressure, MPa
S	calculation parameters
t	time, s
T	temperature, K
u	gas velocity, $m{\cdot}s^{-1}$
V	volume, m^3
x	position, m
$\dot{x}$	velocity, $m{\cdot}s^{-1}$
$\ddot{x}$	acceleration, $m{\cdot}s^{-2}$

Greek symbols

Δp	pressure drop, MPa

Subscripts

b	buffer space
bo	buffer space at a static equilibrium state
c	compression space
d	displacer
co	compression space at a static equilibrium state
e	expansion space
eo	expansion space at a static equilibrium state
h	heater
k	cooler
p	piston
r	regenerator

Acronyms

ANN	artificial neural network
FPSE	free piston Stirling engine
LM	Levenberg-Marguardt
MAPE	mean absolute percentage error
MSE	mean squared error

system [8]. Some researchers focused on predicting the amplitudes of the displacer and piston, and power by considering several nonlinear factors [12–18]. Sim and Kim obtained the dynamic performance of an FPSE based on linear and nonlinear analytical models; Simultaneously, the designed and performance measurements with a nonlinear load damping coefficient were presented, the amplitudes of the displacer and piston were predicted [12,13]. Zare et al. applied a multiple-scale perturbation method to build a thermodynamic–dynamic model with nonlinear springs. Using this method, the frequency, phase angle, pistons amplitudes, and output power were calculated. However, the interactive influences of the thermodynamic and dynamic parameters on the displacements of the displacer and piston are ignored, and it is difficult to find open literature on interactive analyses of the parameters concerning the performance of a nonlinear FPSE system. Moreover, very rarely work has been conducted on the prediction models of nonlinear FPSE systems using both response surface methodology (RSM) and artificial neural networks (ANNs). In addition, there are other factors affecting the performance of the FPSE, and the amount of data processing will increase when all the influences are considered. Therefore, researchers are concerned with finding an effective model that can predict FPSE performance quickly and accurately, which can provide an effective guideline for optimization the FPSE's design. Simultaneously, it is necessary to study on interaction analyses of thermodynamic and dynamic parameters.

RSM is known to be an effective method for predicting the input–output relationships of engineering systems by considering parameter interactions [19–22]. RSM utilises regression techniques to address problems involving the response variables, which are influenced in complex ways. This method can also provide the regression equations of variables and responses from experiments within specific ranges and show the relationships between input and output variables via contour plots. Recently, the RSM and desirability approaches were applied to analyses and optimise the thermodynamic performance of an FPSE, the optimised parameters were obtained for the maximal output power, as well as thermal and exergy efficiencies [23]. Solmaz also applied the RSM to evaluate the effects of working parameters on the performance of a beta-type Stirling engine; the optimum working condition was obtained and specific power was determined using the desirability function method [24].

The ANN method involves comprises interconnected elements named neurons, and has been used widely in function approximation owing to its high capability for modelling nonlinear functions [25,26]. Several researchers have used ANNs to predict the performance of the Stirling engine [26–28]. Yasar et al. developed an ANN model to estimate the power and torque under different operating conditions; based on their results, the ANN model could accurately predict the output values of the Stirling engine [27]. Ahmadi et al. proposed a feed-forward ANN model to predict the Stirling engine's power; their results proved the effectiveness of the ANN model [26]. Ye et al. applied an ANN model to predict the dynamic performance of a beta-type FPSE, and the best architectures for three parameters were achieved through training and testing of the model; their results show that the ANN model is a powerful approach for predicting the FPSE dynamic performance [28].

As seen from the above literature, the RSM and ANN methods have been applied by several researchers to predict the performances of Stirling engines. However, these Stirling engines did not have the free-piston structure [26,27], and the coupling of thermodynamic and dynamic parameters was not considered [23]. In addition, the nonlinear factors of the dynamic equations for two pistons were not included in the dynamic modelling [28]. As noted above, the FPSE is a complex-degree-of-freedom system with many influencing thermodynamic-dynamic parameters, and there are currently no reported studies on the performance prediction of a free-piston Stirling engine by comparison of the ANN and RSM models. Therefore, the aim of this study is to analyse and predict the performance of a nonlinear free-piston Stirling engine using the RSM and ANN models. Five thermodynamic and dynamic parameters, including hot-end temperature, cold-end temperature, load damping, and spring stiffnesses of the displacer and piston, are selected as the input parameters, while the amplitudes of the displacer and piston, operating frequency and output power are selected as the output parameters. In addition, the functions between the input and output parameters are obtained using both the RSM and ANN models. A comparison of these two models is also presented based on the prediction functions of the FPSE. These models provide effective approaches

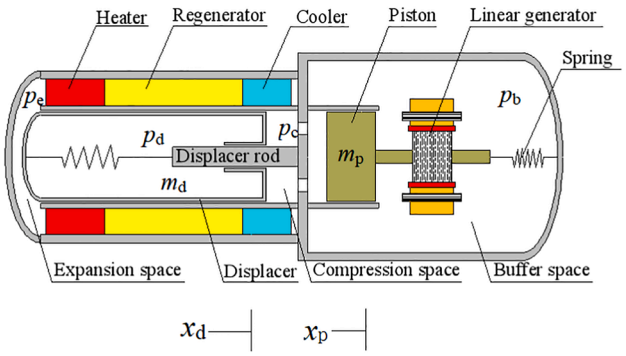

Fig. 1. Schematic of gamma-type FPSE.

for predicting and optimising the FPSE performances accurately and quickly.

2. Model description

Fig. 1 shows the schematic of a gamma-type FPSE, which is a reciprocating resonance system. The displacer and piston are operated in separate cylinders in this type of FPSE. As can be seen in the figure, the FPSE mainly consists of three heat exchangers (heater, regenerator, and cooler), a compression space, an expansion space, a displacer, a piston, and a buffer space. The power piston and displacer are supported by spring stacks, and the model discussed is based on the structure shown in Fig. 1. The purpose of this study is to mainly predict the performance of the FPSE and obtain expressions between the input and output parameters. The basic design parameters of the FPSE used here are derived from that presented in [29] and will not be repeated here.

As shown in Fig. 1, the dynamic system consists of the vibration systems of the displacer and piston, which are acted upon by inertia, damping, spring, load, and internal pressure forces. The equations of motion for the displacer and piston are described using Newton's second law as follows:

$$m_d\ddot{x}_d + c_d\dot{x}_d + k_d x_d = (p_d - p_c)A_r + \Delta p A_d \tag{1}$$

$$m_p\ddot{x}_p + c_p\dot{x}_p + k_p x_p = -F_{load} - (p_b - p_c)A_p \tag{2}$$

In Eq. (2), Δp is defined as a linear expression:$A_d\Delta p = c_{dd}\dot{x}_d + c_{pp}\dot{x}_p$, and F_{load} is described as the nonlinear expression of the load force: $F_{load} = (k_{alt} - k_c x_p^2)\dot{x}_p$.

According to the load damping coefficient k_{alt} and load nonlinear coefficient k_{c}, the output power of the FPSE is expressed as:

$$p_{out} = \frac{1}{2}\omega^2 k_{alt}x_p^2 + \frac{1}{8}\omega^2 k_c x_p^4 \tag{3}$$

The volumes of the expansion and compression spaces are given as:

$$V_e = V_{eo} - A_d x_d \tag{4}$$

$$V_c = V_{co} - A_p x_p + (A_d - A_r)x_d \tag{5}$$

During the FPSE design, the average pressure of the working gas is obtained according to the ideal gas law. The linearised expression for pressure p in thecompression space is approximated by as:

$$p \approx p_m\left(1 + \frac{A_p}{ST_c}x_p - \left(\frac{(A_d - A_r)}{ST_c} - \frac{A_d}{ST_e}\right)x_d\right) \tag{6}$$

$$S = \frac{V_r \ln(T_h/T_k)}{T_h - T_k} + \frac{V_k}{T_k} + \frac{V_h}{T_h} + \frac{V_{eo}}{T_e} + \frac{V_{co}}{T_c} \tag{7}$$

According to Fig. 1, the volume of the buffer space V_{b} is:

$$V_b = V_{bo} + A_p x_p \tag{8}$$

Thus, the pressure of the buffer space is written as:

$$p_b = p_m(1 + \frac{A_p}{V_{bo}}x_p)^{-\gamma} = p_m - \frac{\gamma p_m A_p}{V_{bo}}x_p \tag{9}$$

Combining the above equations, the dynamic equation of a nonlinear FPSE system is expressed in the form of a state-space, equation as follows:

$$\dot{X} = MX + f\left(X\right) \tag{10}$$

$$\dot{X} = \begin{bmatrix} \dot{x}_1 \\ \dot{x}_2 \\ \dot{x}_3 \\ \dot{x}_4 \end{bmatrix}, X = \begin{bmatrix} x_1 \\ x_2 \\ x_3 \\ x_4 \end{bmatrix} \tag{11}$$

$$M = \begin{bmatrix} 0 & 1 & 0 & 0 \\ K_{\mathrm{dd}} & D_{\mathrm{dd}} & K_{\mathrm{dp}} & D_{\mathrm{dp}} \\ 0 & 0 & 0 & 1 \\ K_{\mathrm{pd}} & D_{\mathrm{pd}} & K_{\mathrm{pp}} & -\frac{k_{\mathrm{alt}} + c_{\mathrm{p}}}{m_{\mathrm{p}}} \end{bmatrix}, f(X) = \begin{bmatrix} 0 \\ 0 \\ 0 \\ \frac{k_{\mathrm{c}}}{m_{\mathrm{p}}}x_3^2 x_4 \end{bmatrix} \tag{12}$$

$$x_1 = x_d, x_2 = \dot{x}_d, x_3 = x_p, x_4 = \dot{x}_p \tag{13}$$

Then, K_{dd}, K_{dp}, K_{pp}, K_{pd}, D_{dd}, D_{dp}, D_{pp}, and D_{pd} are obtained as follows:

$$K_{dd} = -\frac{p_m A_p^2}{m_p}\left(\frac{\gamma}{V_{bo}} + \frac{1}{ST_c} + \frac{k_p}{p_m A_p^2}\right), K_{dp} = -\frac{p_m A_r A_p}{m_d S T_c} \tag{14}$$

$$K_{pp} = \frac{p_m A_p^2}{m_p}\left(\frac{\gamma}{V_{bo}} - \frac{1}{ST_c} - \frac{k_p}{p_m A_p^2}\right), K_{pd} = \frac{p_m A_p}{m_p S}\left(\frac{A_d - A_r}{T_c} - \frac{A_d}{T_e}\right) \tag{15}$$

$$D_{dd} = -\frac{c_d - c_{dd}}{m_d}, D_{dp} = \frac{c_{pp}}{m_d} \tag{16}$$

$$D_{pp} = -\frac{c_p + k_{alt}}{m_p}, D_{pd} = 0 \tag{17}$$

3. Brief descriptions of RSM and ANN

3.1. Response surface methodology

In this section, the simulation experiment designs based on the RSM are presented using the Design expert 8.0.6.1 software to obtain a prediction model of the FPSE. The aim here is to build a suitable approximation of the relationship between the thermodynamic–dynamic parameters and the four responses via the RSM method. Eq. (18) shows the regression model that considers the interactions between the input and output parameters [30].

$$y = \chi_0 + \sum_{i=1}^{k}\chi_i x_i + \sum_{i=1}^{k-1}\sum_{j=2}^{k}\chi_{ij}x_i x_j + \sum_{i=1}^{k}\chi_{ii}x_i^2 \tag{18}$$

where y is the response variable; k is the number of variables; x_{i} and x_{j} are the independent factors (e.g., hot-end temperature, cold-end temperature); χ_0 is the intercept term; χ_{i}, χ_{ii} and χ_{ij} ($i = 0, 1, 2,\ldots, k; j = i + 1, 1, 2,\ldots, k$) are the regression coefficients for the linear, quadratic and interaction terms respectively.

It is necessary to design simulations that can provide sufficient variables to predict the regression coefficients in Eq. (18). The Box–Behnken design (BBD) is applied to generate the simulation matrix owing to its fewer design points because the number of factors is less. The input variables are the hot-end temperature, cold-end temperature, coefficient of load damping, and spring stiffnesses of the displacer and

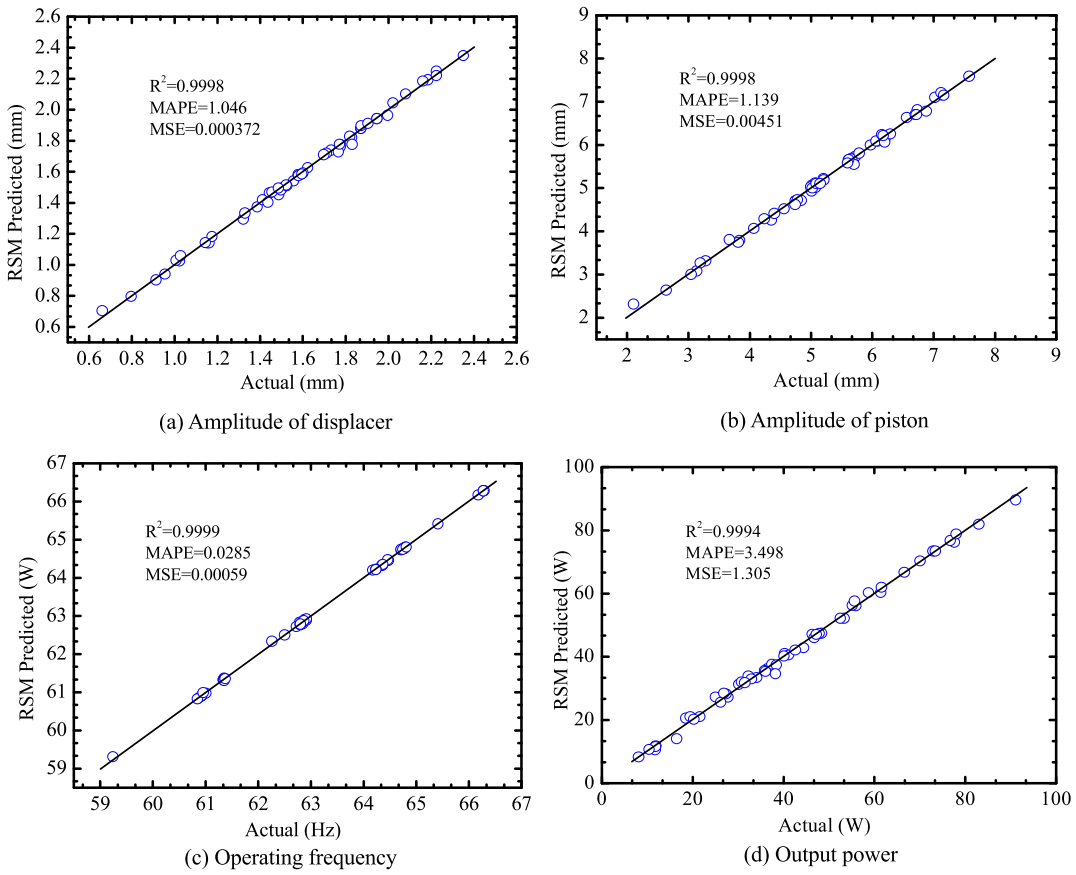

Fig. 2. RSM predictions versus actual results.

piston, which influence the performance of FPSE greatly, while the output variables are the amplitudes of the displacer and piston, operating frequency, and output power. The ranges of the input parameters are mainly based on actual engineering design. According to the established variables, responses, and ranges of variables, the four response results from the five thermodynamic–dynamic parameters of the FPSE by the BBD are obtained. Some additional design points are added to ensure accuracy of the quadratic regression model. Thus, a total of fifty-five simulation experiments were performed. The design of the simulations using RSM is shown in Appendix B; the run numbers of the experiments are shown in the first column, the next five columns indicate the parameter combinations, and last the four columns to the right show the responses. There are three main analytical steps, including the analysis of variance (ANOVA), regression model of the responses, and sensitivity analyses of the different variables.

3.2. Artificial neural networks

Recently, ANNs technology have been widely used in various fields [31–33]. ANN models typically consist of three main layers, namely the input, hidden, and output layers, with specific numbers of neurons in each layer. Two types of functions, namely summation and activation functions, are used for each layer. The summation function is used to obtain the net input of a cell, and the activation function, which determines the output of the cell, provides a suitable match between the input and output layers.

The selection of the activation function is based on the type of the neural network. Generally, a sigmoid function is adopted as the transfer function of the ANN model owing to its continuous and nonlinear properties, as shown in the following equations:

$$f(Net_i) = \frac{1}{1 + e^{-Net_i}} \tag{19}$$

$$Net_i = \sum_{j=1}^{n} w_{ij} x_j + wb_i \tag{20}$$

In most applications, the back propagation (BP) neural network structure with the Levenberg–Marquardt (LM) algorithm is usually adopted for its strong nonlinear mapping ability [34,35]. Therefore, the BP neural network with LM training function is thus used in this work. The ANN model used herein was developed with Matlab–R2016a software.

The performances of the RSM and ANN models can be evaluated using statistical methods for the mean absolute percentage error (MAPE), mean-squared error (MSE), and correlation coefficient (R^2) for the purpose of comparison [36,37]; these parameters can be defined as follows:

$$MAPE = \frac{1}{n} \sum_{m=1}^{n} \frac{\left| y_{act,m} - y_{pre,m} \right|}{y_{act,m}} \times 100 \tag{21}$$

$$MSE = \frac{1}{n} \sum_{m=1}^{n} \left(y_{act,m} - y_{pre,m} \right)^2 \tag{22}$$

$$R^2 = 1 - \frac{\sum_{m=1}^{n} \left(y_{pre,m} - y_{act,m} \right)^2}{\sum_{m=1}^{n} \left(y_{act,m} \right)^2} \tag{23}$$

where n is the number of data, and $y_{act,m}$ and $y_{pre,m}$ are the actual and predicted values, respectively.

In general, the value of R^2 varies from 0 to 1; a value close to 1

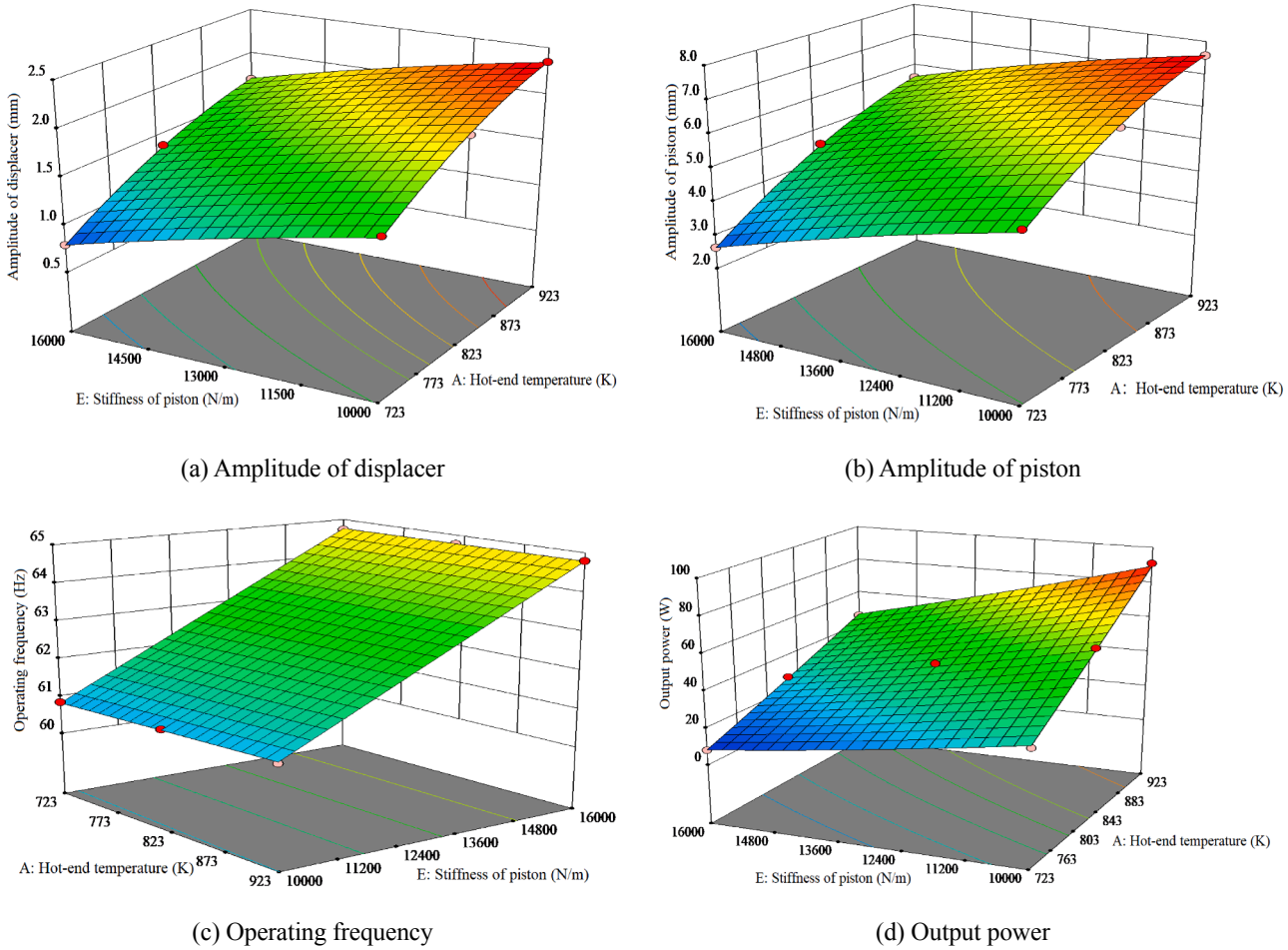

(a) Amplitude of displacer

(b) Amplitude of piston

(c) Operating frequency

(d) Output power

Fig. 3. Interactive effects of hot-end temperature and stiffness of piston on the output parameters.

indicates that there is a positive linear correlation between the network output and target value, and a value close to 0 implies weak or no correlation.

4. Results and discussion

4.1. RSM analysis

4.1.1. Analysis of variance (ANOVA)

The ANOVA, also known as the "analysis of variance test", is the most efficient method to evaluate the accuracy between the the experimental and predicted models. The results of ANOVA are indicated in Appendix C. The p value is a measure of the difference between the obtained and observed results in statistics. If the p value is less than 0.05, the factors show significance for all four responses, meaning that the model can be applied to predict results accurately. It can be seen from Appendix C, that the main effects of the hot-end temperature (X_1), cold-end temperature (X_2), coefficient of load damping (X_3), and spring stiffnesses of the displacer and piston (X_4 and X_5), as well as their interactions X_1X_2, X_1X_3, X_1X_5, X_2X_3, X_3X_4, X_3X_5, and X_4X_5, and quadratic terms X_1^2,X_4^2, andX_5^2 are significant for the amplitude of the displacer (X_d). Other quadratic and interaction terms with larger p value have minor effects on X_d and X_p. Based on the p values, X_1, X_2, X_4, X_5, X_1X_4, X_1X_5, X_2X_4, and X_4X_5 are significant on for f. For the output parameter -p_{out}, the parameters X_1, X_2, X_3, X_4, X_5, X_1X_4, X_1X_5, X_2X_3, X_2X_4, X_2X_5, X_4X_5, X_2^2, X_3^2, andX_5^2 are significant.

4.1.2. Regression equations of responses

Based on the 55 simulation results presented in Appendix B, the regression models were proposed using RSM for the amplitudes of the displacer and piston, operating frequency, and output power as functions of the five selected parameters given the limits of each of the factors. The calculated equations for the variables are given in Appendix D.

The deviations for X_d, X_p, f, and p_{out} from the previous model and the regression models are indicated in Fig. 2. As shown in Fig. 2, most of the predicted points are distributed along the diagonal lines. The R^2 for X_d, X_p, f, and p_{out} are 0.9998, 0.9998, 0.9999, and 0.9994, respectively, while the mean absolute percentage and mean absolute error values for the four responses are very low. In addition, the deviations between the actual results and values predicted by the RSM for X_d, X_p, f, and p_{out} are within 10% margins of error, meaning that the regression model can predict these results accurately.

For the RSM analyses, 3D surface plots are used to show the interactive effects of these two input factors and evaluate the influences of two parameters on the FPSE performance. According to the p values in Appendix C, the interactions of X_1X_5 and X_4X_5 have significant influences on the amplitudes of the displacer and piston, operating frequency, and output power; thus, these two sets of interactions are studied in detail, as shown in Fig. 3 and Fig. 4.

4.1.3. Interactive effects analysis

Two sets of 3D surface plots are drawn using RSM to study the interactions of the different independent parameters. Fig. 3 shows the interactive effects of the hot-end temperature and stiffness of piston on

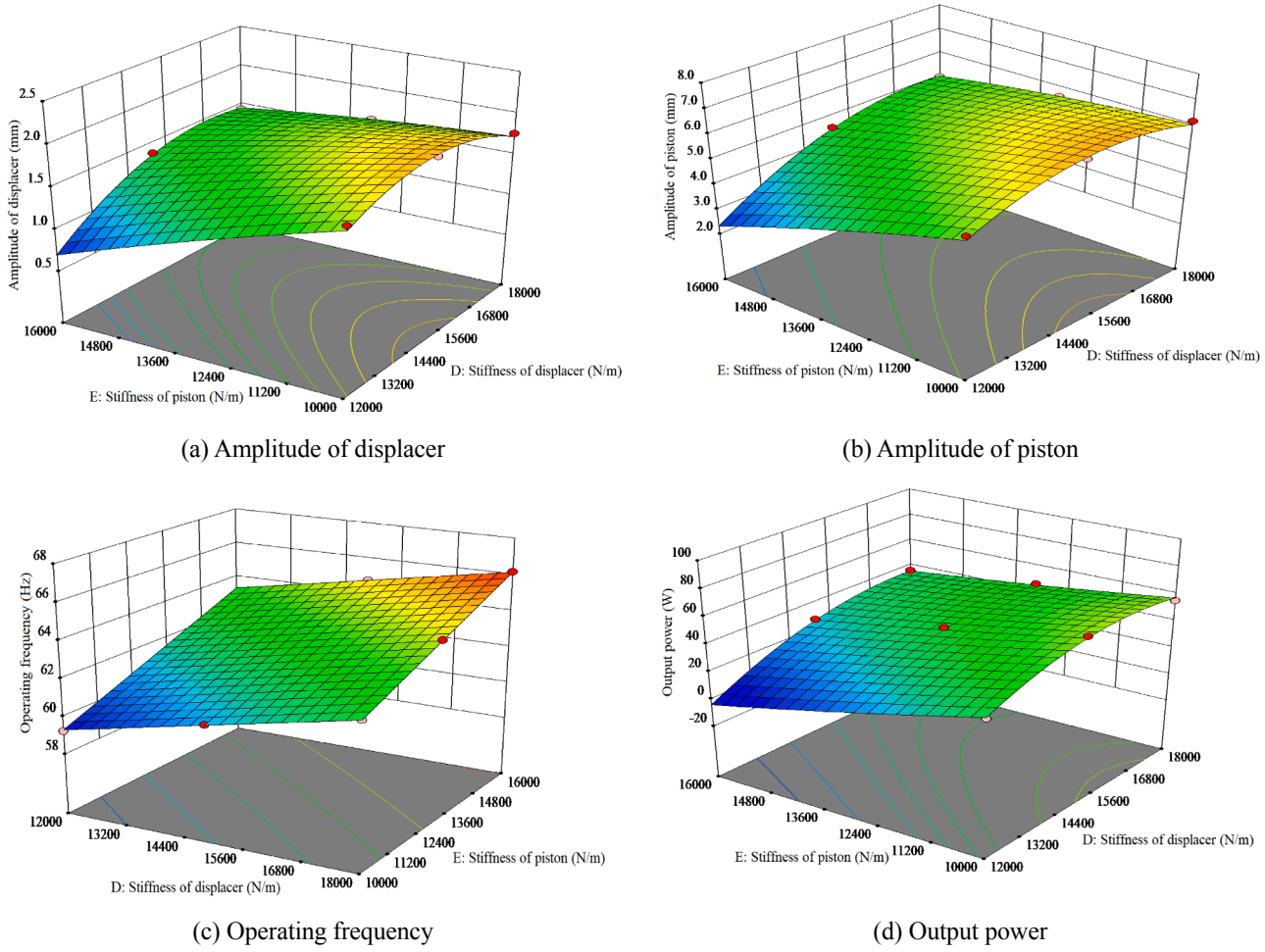

(a) Amplitude of displacer (b) Amplitude of piston

(c) Operating frequency (d) Output power

Fig. 4. Interactive effects of stiffnesses of the two pistons springs on the output parameters.

the amplitudes of the displacer and piston, operating frequency, and output power. In the analysis, the cold-end temperature, coefficient of load damping, and spring stiffness of displacer are 300.5 K, 13.0 Ns/m, and 1.5 × 10^4N/m, respectively. It can be seen from Fig. 3(a) and Fig. 3 (b) that the amplitudes of the displacer and piston increase with the hot-end temperature. As the spring stiffness of the piston decreases, the amplitudes of the two pistons increase. Moreover, the maximal amplitudes of the two pistons can be obtained by decreasing their spring stiffnesses and increasing the hot-end temperature. The interactive influences of the hot-end temperature and spring stiffness of the piston on the operating frequency are presented in Fig. 3(c). It can be seen that the operating frequency increases proportionally with the pistonspring stiffness. In addition, the spring stiffness has a larger effect than the hot-end temperature. This is because the operating frequency is determined by the masses and spring stiffnesses of the two pistons based on the theory of vibration. Although the hot-end temperature affects the operating frequency, it is not the main factor. As seen in Fig. 3(d), the output power increases linearly with the hot-end temperature when the piston stiffness is fixed to 10000 N/m; and for a hot-end temperature of 923 K, the maximal output power is 90.2 W.

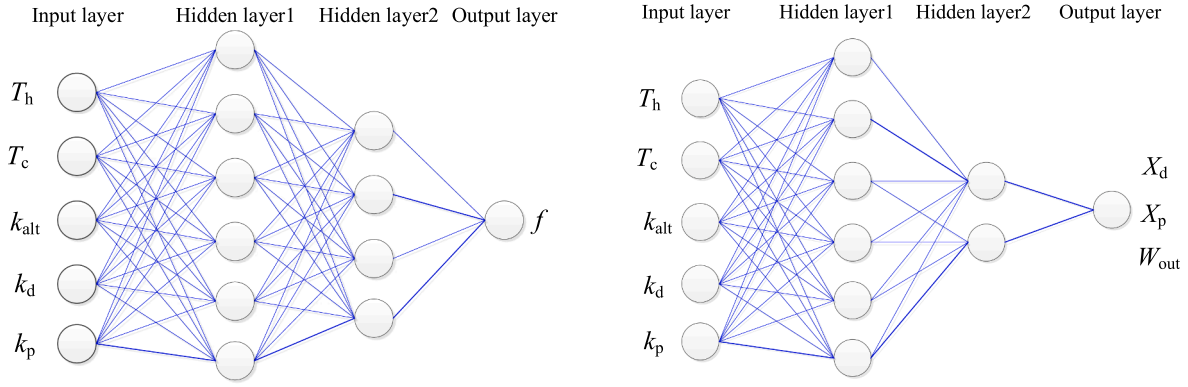

（a）Operating frequency (b) Amplitudes of displacer and piston and output power

Fig. 5. ANN models with two hidden layers for the four parameters of the FPSE.

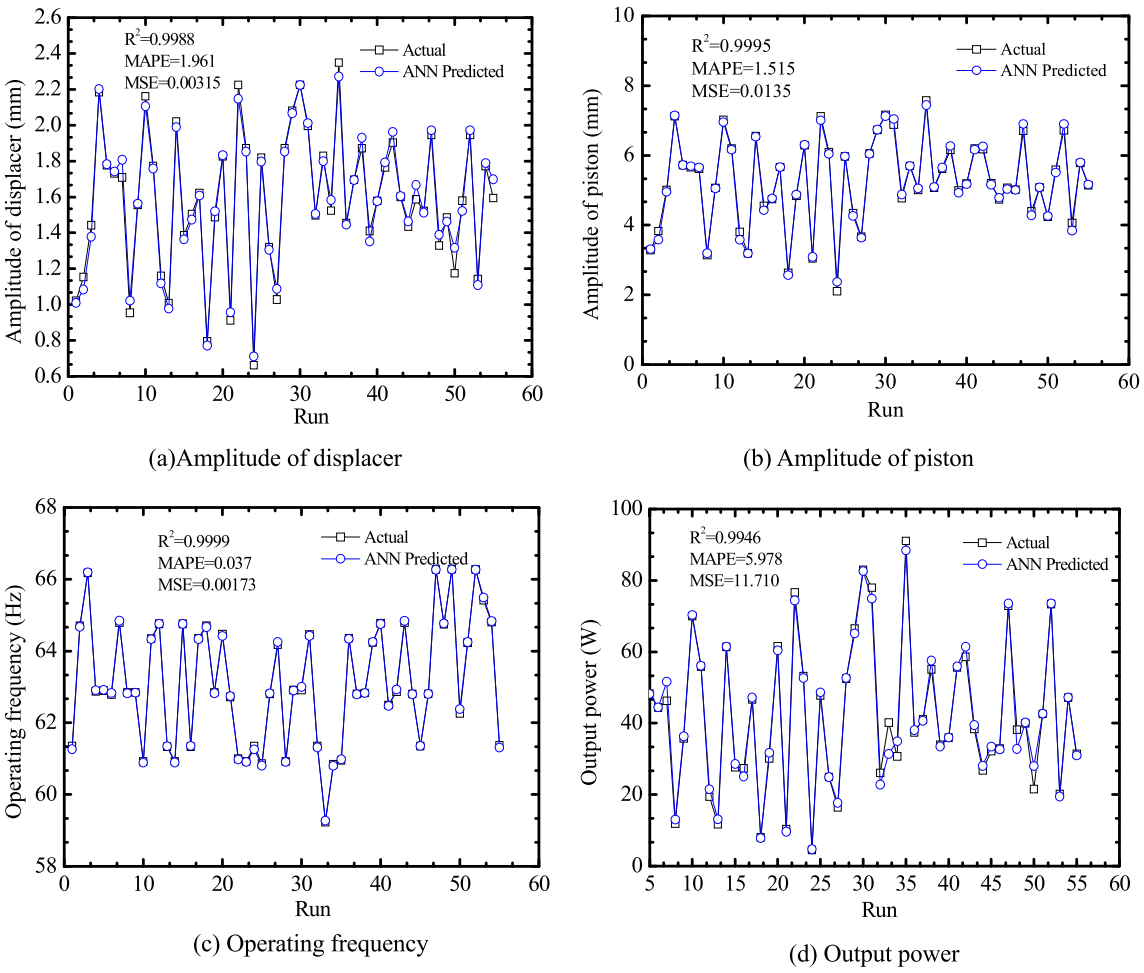

Fig. 6. ANN predictions versus actual results.

Fig. 4 indicates the interactive influences of the spring stiffnesses of the displacer and piston on the amplitudes of the displacer and piston, operating frequency, and output power. The hot-end temperature, cold-end temperature, and coefficient of load damping are 823 K, 300.5 K, and 13.0 Ns/m, respectively. As seen from Fig. 4(a) and Fig. 4(b), as the spring stiffness of the displacer increases, the amplitudes of the displacer and piston increase and display nonlinear variations. For a small value of the spring stiffness of the piston, the amplitudes of the displacer and piston increase with the spring stiffness of the displacer while operating frequency increases linearly with the spring stiffnesses of the two pistons (shown in Fig. 4(c)). The frequency reaches 66.2 Hz as the stiffnesses of the displacer and piston is 18000 N/m and 16000 N/m, respectively. This is because the operating frequency is proportional to the spring stiffnesses of the two pistons, and can be increased by adjusting the spring stiffnesses of the two pistons. However, the increase in the spring stiffnesses result in the instability and nonlinear phenomena of the FPSE system; thus, the appropriate spring stiffness should be selected for a reasonable range of design. As seen in Fig. 4(d), the output power increases with the stiffness of the displacer. It should be noted that a small spring stiffness of the piston and large stiffness of the displacer can increase output power.

4.2. ANN analysis

4.2.1. ANN architecture

Generally, it is of great importance to design suitable ANN architectures and algorithms to ensure the accuracy of the predicted values. Following a series of trials, the best results were observed to be obtained by applying six neurons in the first hidden layer. The architectures of the ANN with hidden layers for amplitudes of the displacer and piston, operating frequency, and output power are illustrated in Fig. 5. It is seen that models with LM 5–6-2–1 are the ANN structures of X_d, X_p, and p_{out} while that with LM 5–6-4–1 is the network architecture of f.

The comparison results between the actual and predicted ANN values for the amplitudes of the displacer and piston, operating frequency, and output power are shown in Fig. 6(a)–(d). It is seen that the values of R^2 for X_d, X_p, f, and p_{out} are 0.9988, 0.9995, 0.9999, and 0.9946, respectively. The MSE and MAPE values of X_d, X_p, and f are <0.01 and 5 while those of p_{out} are 5.978 and 11.71. It can also be seen that about 95% of the parameters are accurately predicted by the ANN with $<10\%$ error, meaning that there is good agreement between the four output parameters and their predicted values. Therefore, the predictions of the ANN model are satisfactory.

4.2.2. Expressions of the output parameters using ANN model

Based on the analysis of the ANN model, the expressions of the amplitudes of the displacer and piston, operating frequency, and output power are shown in Eqs. (24) and (27); the expressions M_i for X_d, X_p, f, and p_{out} are the activation functions, the weights are presented in Appendixes 5–8E-H. According to the ANN architectures in Fig. 5, the activation functions F_i for X_d, X_p, f, and p_{out} are obtained by applying the weights between the first and second hidden layers after applying the N_j functions that are the weights between the input and first hidden layers. It is possible to observe the effects of these parameters from the following equations:

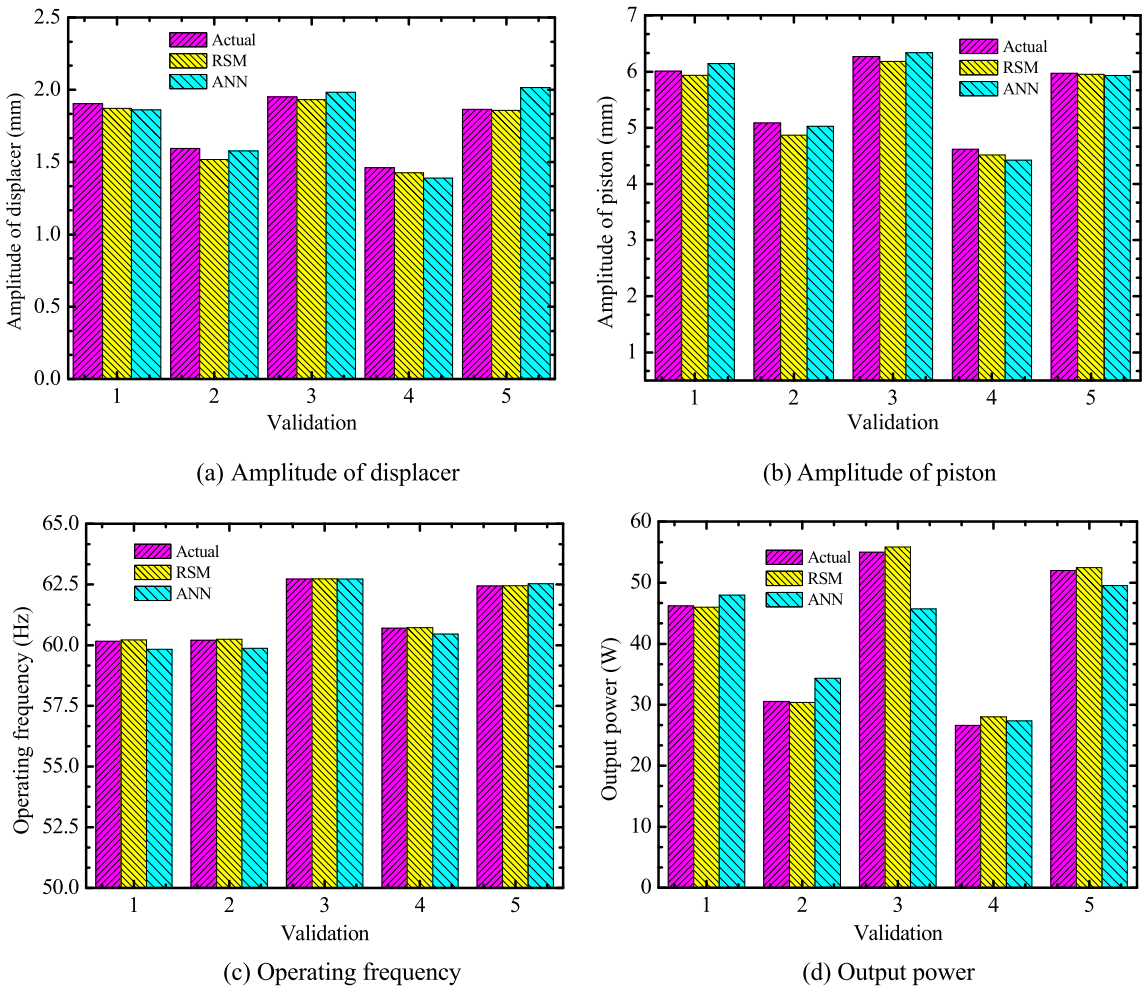

Fig. 7. Actual results vs. the ANN and RSM predictions.

$$X_d = \frac{1}{1 + e^{-(0.304 \times M_1 - 0.8677 \times M_2 - 0.4491)}} \tag{24}$$

$$X_p = \frac{1}{1 + e^{-(-0.2821 \times M_1 - 0.2737 \times M_2 + 0.4651)}} \tag{25}$$

$$f = \frac{1}{1 + e^{-(0.0994 \times M_1 + 0.8344 \times M_2 - 0.4283 \times M_3 + 0.5144 \times M_4 - 0.5075)}} \tag{26}$$

$$p_{out} = \frac{1}{1 + e^{-(0.3112 \times M_1 + 0.8764 \times M_2 + 0.2409)}} \tag{27}$$

4.3. Comparison of the predicted values using ANN and RSM models

The performance of the FPSE was predicted by the RSM and ANN methods, as detailed in Sections 4.1 and 4.2. In addition, the expressions of the amplitudes of the displacer and piston, operating frequency and output power were derived. The predicted parameters obtained from the RSM and ANN models were compared with the actual simulations to evaluate the accuracies of the two models. From Fig. 2 and Fig. 6, it is seen that R^2 values for the RSM models of the responses are higher than those of the ANN models. To further verify the prediction models, five sets of parameters were selected for comparison, as shown in Fig. 7. It is evident from Fig. 7 that the deviations between the predicted RSM and actual values are very small compared to those of the ANN models. Around 95% of the data for X_d, X_p, f, and p_{out} from iterations 1 to 5 are predicted by the RSM with errors $< 5\%$. However, the error of the output power of iteration of 3 for the ANN model exceeds 10%, meaning that the overall error of the RSM was less than that of the ANN. The higher values for R^2, MAPE, and MSE, as well as the figures for the predicted and actual values show that the RSM model is more accurate than the ANN model.

5. Conclusions

Two efficient and highly accurate prediction tools, namely response surface methodology and artificial neural network, were applied to analysis and predict the performance of a gamma-type free piston Stirling engine. The analysis of variance was adopted as the statistical procedure to assess the effects and significances of the thermodynamic and dynamic parameters on the amplitudes of the displacer and piston, operating frequency, and output power. The relationship between the input and output parameters was determined using these two models. The results of these analyses are summarized as follows:

(1) During the analysis of response surface methodology model, the regression models for the amplitudes of the displacer and piston, operating frequency, and output power were obtained and evaluated for accuracy. Two sets of interactions of the Stirling engine's thermodynamic and dynamic parameters that had significant effects on the four output parameters were studied in detail. The results show that good fit was achieved and that the model had good accuracy. The selected input parameters had statistically significant impacts on the performance, and the amplitudes of the two pistons, operating frequency, and output

power increased with the hot-end temperature and stiffness of the displacer spring.

(2) The deviation analyses between the actual and predicted values for both methods were evaluated via comparisons of their mean absolute percentage error, mean-squared error, and correlation coefficients. The results indicated that the R^2 values for the amplitudes of the displacer and piston, operating frequency, and output power were 0.9998, 0.9998, 0.9999 and 0.9994, respectively, using the model of response surface methodology, and that these values were all higher than those calculated using the model of artificial neural network. The results showed that the response surface methodology model is more accurate than the artificial neural network model.

(3) Five validation parameters were selected to further verify and compare the prediction models. The results showed that the deviations between the predicted by response surface methodology and actual values were very small compared to those of the artificial neural network model. Around 95% of the data for the four output parameters were predicted by the response surface methodology with errors $< 5\%$, indicating that the response surface methodology model is more accurate than the artificial neural network model.

According to these results, this study makes significant contributions in the following areas: (1) The interactive influences of selected input parameters that have significant effects on the amplitudes of the displacer and piston, operating frequency, and output power are analysed, so that the performance can be improved by adjusting multiple parameters simultaneously. (2) The relationship between the input and output parameters was achieved by using two effective methods, indicating that reliable predictive models can be implemented effectively to optimise and predict the performance of the Stirling engine accurately and quickly. In our future work, we intend performing experimental investigations based on the results predicted by these two models. Moreover, it is necessary to conduct multi-objective optimization of the performance of the nonlinear free piston Stirling engine by adjusting its thermodynamic and dynamic parameters.

Declaration of Competing Interest

The authors declare that they have no known competing financial interests or personal relationships that could have appeared to influence the work reported in this paper.

Acknowledgements

This work is financially supported by Key Laboratory of Vacuum Technology and Physics Foundation of China (No. 6142207020901) and the National Natural Science Foundation of China (No. 51976146).

Appendix A. . Prior research on dynamic performance of FPSE

Authors	Model/methods	Summary of conclusion
Rogdakis et al. [8]	Linear	A mathematical form for frequency, phase angle and amplitude ratio
Karabulut et al. [9]	Linear	A stable operation within small ranges for the hot-end temperature and piston damping coefficient
Kwankaomeng et al. [10]	Linear	Obtain the stability of engine operation over the frequency range of 6.2– 6.4 Hz
Khripach et al [11]	Linear	Determine the parameters of two pistons and the range of load
Sim et al. [12,13]	Linear and nonlinear	Predict the amplitudes of the displacer and piston by considering the damping of external load
Ulusoy [14]	Nonlinear	Achieve the influences of nonlinear load, nonlinear pressure loss and the nonlinear spring on the performance of the FPSE
Tavakolpour et al. [15]	Nonlinear/ perturbation technique	Obtain the relationships to predict frequency, phase, pistons strokes, power, and efficiency
Zare et al [16]	Nonlinear/ perturbation technique	Achieve damping coefficients of the displacer and piston
Cascella et al. [17]	Nonlinear/ equivalent electrical circuit	Predict the frequency, piston stoke, and compression pressure amplitude
Majidniya et al. [18]	Linear and nonlinear	Develop a linear and nonlinear model and obtain a combined system of a Stirling engine with a generator

Appendix B. . Design of experiment using RSM

Run	Factors					Responses			
	T_h (K)	T_c (K)	k_{alt} (Ns/m)	k_d (N/m)	k_p (N/m)	x_d (mm)	x_p (mm)	f (Hz)	p_{out} (W)
1	823	313.0	13	12,000	13,000	1.023	3.283	61.35	11.71
2	823	313.0	13	15,000	16,000	1.153	3.832	64.71	18.45
3	823	300.5	13	18,000	16,000	1.443	5.015	66.18	36.47
4	923	300.5	12	15,000	13,000	2.184	7.120	62.88	77.57
5	823	288.0	14	15,000	13,000	1.777	5.720	62.90	48.31
6	823	300.5	13	15,000	13,000	1.732	5.656	62.79	44.40
7	923	300.5	13	15,000	16,000	1.710	5.613	64.79	46.28
8	723	300.5	14	15,000	13,000	0.955	3.137	62.85	11.85
9	823	300.5	14	15,000	13,000	1.556	5.070	62.85	35.79
10	823	300.5	12	15,000	10,000	2.161	7.019	60.92	70.00
11	823	300.5	12	18,000	13,000	1.773	6.203	64.35	55.89
12	823	300.5	14	15,000	16,000	1.161	3.811	64.76	19.45
13	823	300.5	14	12,000	13,000	1.007	3.195	61.34	11.78
14	823	300.5	13	15,000	10,000	2.021	6.561	60.92	61.37
15	823	300.5	13	15,000	16,000	1.386	4.560	64.76	27.75
16	823	288.0	13	12,000	13,000	1.505	4.743	61.34	27.36
17	823	300.5	13	18,000	13,000	1.622	5.663	64.36	46.71
18	723	300.5	13	15,000	16,000	0.796	2.636	64.71	8.07
19	723	288.0	13	15,000	13,000	1.487	4.838	62.85	30.13

(*continued on next page*)

(*continued*)

Run	Factors					Responses			
	T_h (K)	T_c (K)	k_{alt} (Ns/m)	k_d (N/m)	k_p (N/m)	x_d (mm)	x_p (mm)	f (Hz)	p_{out} (W)
20	823	288.0	13	18,000	13,000	1.827	6.293	64.47	61.55
21	723	313.0	13	15,000	13,000	0.913	3.044	62.72	10.35
22	823	288.0	13	15,000	10,000	2.224	7.119	61.00	76.66
23	823	300.5	14	15,000	10,000	1.871	6.095	60.92	53.27
24	723	300.5	13	12,000	13,000	0.662	2.104	61.35	4.49
25	823	313.0	13	15,000	10,000	1.818	5.969	60.86	47.79
26	823	313.0	14	15,000	13,000	1.321	4.348	62.80	25.01
27	723	300.5	13	18,000	13,000	1.028	3.669	64.17	16.43
28	823	300.5	14	15,000	10,000	1.872	6.059	60.92	52.47
29	823	288.0	12	15,000	13,000	2.080	6.732	62.91	66.56
30	923	288.0	13	15,000	13,000	2.224	7.163	62.91	82.97
31	923	300.5	13	18,000	13,000	1.996	6.878	64.46	77.97
32	823	300.5	12	12,000	13,000	1.498	4.775	61.35	26.12
33	823	300.5	13	12,000	10,000	1.83	5.700	59.24	40.22
34	723	300.5	13	15,000	10,000	1.524	5.009	60.84	30.74
35	923	300.5	13	15,000	10,000	2.235	7.578	60.96	91.04
36	823	300.5	14	18,000	13,000	1.455	5.068	64.36	37.45
37	823	313.0	12	15,000	13,000	1.697	5.616	62.80	41.08
38	923	313.0	13	15,000	13,000	1.872	6.153	62.83	55.11
39	823	313.0	13	18,000	13,000	1.411	4.995	64.23	34.02
40	823	300.5	12	15,000	16,000	1.578	5.203	64.78	36.01
41	823	300.5	13	18,000	10,000	1.766	6.198	62.50	55.58
42	923	300.5	14	15,000	13,000	1.904	6.175	62.87	58.66
43	823	288.0	13	15,000	16,000	1.601	5.209	64.79	38.38
44	723	300.5	12	15,000	13,000	1.436	4.739	62.80	26.87
45	923	300.5	13	12,000	13,000	1.601	5.071	61.35	32.21
46	823	313.0	13	15,000	13,000	1.436	5.020	62.80	32.92
47	923	300.5	12	18,000	16,000	1.588	6.699	66.27	72.88
48	923	313.0	14	15,000	16,000	1.522	4.400	64.74	38.20
49	823	288.0	14	18,000	16,000	1.946	5.082	66.29	40.04
50	723	300.5	13	18,000	10,000	1.329	4.238	62.26	21.57
51	823	313.0	12	18,000	13,000	1.485	5.595	64.23	42.57
52	923	300.5	12	18,000	16,000	1.175	6.715	66.27	73.35
53	723	300.5	12	18,000	15,000	1.579	4.066	65.41	20.22
54	823	288.0	12	15,000	16,000	1.946	5.782	64.81	47.16
55	923	313.0	12	12,000	13,000	1.143	5.146	61.37	31.44

Appendix C. . Analysis of variance of the RSM model for different output parameters

Source	p value-X_d	p value- X_p	p value-f	p value-p_{out}
Model	<0.0001*	<0.0001*	<0.0001*	<0.0001*
X_1	<0.0001	<0.0001	<0.0001	<0.0001
X_2	<0.0001	<0.0001	<0.0001	<0.0001
X_3	<0.0001	<0.0001	0.8731	<0.0001
X_4	<0.0001	<0.0001	<0.0001	<0.0001
X_5	<0.0001	<0.0001	<0.0001	<0.0001
X_1X_2	<0.0001	<0.0001	0.2890	0.0719
X_1X_3	<0.0001	<0.0001	0.1813	0.7623
X_1X_4	0.2200	0.0523	<0.0001	<0.0001
X_1X_5	0.0481	0.0153	0.0080	<0.0001
X_2X_3	0.0233	0.0175	0.7479	0.0094
X_2X_4	0.1025	0.2712	<0.0001	0.0001
X_2X_5	0.4604	0.1988	0.2624	<0.0001
X_3X_4	0.0002	0.0033	0.3104	0.0635
X_3X_5	0.0007	0.0008	0.8288	0.0822
X_4X_5	<0.0001	<0.0001	<0.0001	<0.0001
X_1^2	<0.0001	<0.0001	–	0.3195
X_2^2	0.4085	0.2770	–	0.0010
X_3^2	0.1099	0.1471	–	0.0487
X_4^2	<0.0001	<0.0001	–	<0.0001
X_5^2	0.0009	0.0009	–	0.0577
Lack of Fit	0.0004*	0.0489*	–	0.0918 (not significant)

Appendix D. . Equations for X_d, X_p, f, and p_{out}

Equation for amplitude of displacer (mm)

$$X_d = 1.36 + 2.50\times10^{-3}\times T_h\text{-}9.82\times10^{-3}\times T_c + 0.24\times k_{alt} + 3.89\times10^{-4}\times k_d\text{-}2.10\times10^{-4}\times k_p + 4.50\times10^{-5}\times T_h\times T_c\text{+}4.4910^{-4}\times T_h\times k_{alt} + 4.02\times10^{-8}\times T_h\times k_d + 6.86\times10^{-8}\times T_h\times k_p\text{-}1.75\times10^{-3}\times T_c\times k_{alt} + 4.76\times10^{-7}\times T_c\times k_d - 2.06\times10^{-7}\times T_c\times k_p + 1.35\times10^{-5}\times k_{alt}\times k_d\text{-}1.12\times10^{-5}\times k_{alt}\times k_p + 2.25\times10^{-8}\times k_d\times k_p\text{-}1.15\times10^{-5}\times T_h^2 - 4.38\times10^{-5}\times T_c^2\text{-}0.013\times k_{alt}^2\text{-}3.24\times10^{-8}\times k_d^2\text{-}3.41\times10^{-8}\times k_p^2$$

Equation for amplitude of piston (mm)

(*continued on next page*)

(*continued*)

Equation for amplitude of displacer (mm)
X_p = -5.48 + 1.24 × 10^{-3} × T_h + 0.019 × T_c + 1.08 × k_{alt} + 1.25 × 10^{-3} × k_d-3.41 × 10^{-4} × k_p + 1.62 × 10^{-4} × T_h × T_c+1.48 × 10^{-3} × T_h × k_{alt} + 2.25 × 10^{-7} × T_h × k_d + 2.97 × 10^{-7} × T_h × k_p-6.42 × 10^{-3} × T_c × k_{alt} + 1.10 × 10^{-6} × T_c × k_d−1.26 × 10^{-6} × T_c × k_p + 3.59 × 10^{-5} × k_{alt} × k_d-3.83 × 10^{-5} × k_{alt} × k_p + 6.20 × 10^{-5} × k_d × k_p-3.78 × 10^{-5} × T_h^2−2.01 × 10^{-4} × T_c^2-0.040 × k_{alt}^2-9.22 × 10^{-8} × k_d^2-1.19 × 10^{-8} × k_p^2
Equation for operating frequency (Hz)
f = 42.64–3.77 × 10^{-3} × T_h + 0.011 × T_c + 0.16 × k_{alt} + 8.58 × 10^{-4} × k_d + 7.91 × 10^{-4} × k_p + 1.10 × 10^{-5} × T_h × T_c−1.53 × 10^{-4} × T_h × k_{alt} + 2.86 × 10^{-7} × T_h × k_d-1.02 × 10^{-7} × T_h × k_p-2.75 × 10^{-4} × T_c × k_{alt}-1.68 × 10^{-6} × T_c × k_d+3.64 × 10^{-7} × T_c × k_p + 3.91 × 10^{-6} × k_{alt} × k_d-7.55 × 10^{-7} × k_{alt} × k_p-1.08 × 10^{-8} × k_d × k_p
Equation for output power (W)
p_{out} = 1697.84 + 0.23 × T_h-8.39 × T_h-68.47 × k_{alt} + 0.037 × k_d-0.035 × k_p-9.92 × 10^{-4} × T_h × T_c+1.73 × 10^{-3} × T_h × k_{alt} + 2.76 × 10^{-5} × T_h × k_d-1.56 × 10^{-5} × T_h × k_p + 0.12 × T_c × k_{alt}-7.20 × 10^{-5} × T_c × k_d+8.39 × 10^{-5} × T_c × k_p-3.71 × 10^{-4} × k_{alt} × k_d + 3.17 × 10^{-4} × k_{alt} × k_p + 6.50 × 10^{-7} × k_d × k_p + 4.79 × 10^{-5} × T_h^2+0.011 × T_c^2 + 0.93 × k_{alt}^2-1.22 × 10^{-6} × k_d^2 + 1.09 × 10^{-7} × k_p^2

Appendix E. . Weights among layers for amplitude of displacer

$$M_i = \frac{1}{1+e^{-(w_1\times N_1+w_2\times N_2+w_3\times N_3+w_4\times N_4+w_5\times N_5+w_6\times N_6\ +\ \delta_i)}}$$

i	w_1	w_2	w_3	w_4	w_5	w_6	δ_i
Weights between first and second hidden layers for amplitude of displacer							
1	0.0466	0.924	−0.9395	0.0394	0.7801	−0.5406	−0.3782
2	−0.4802	0.0804	0.3926	−0.8819	−0.3396	−0.7721	−0.5431

$$N_j = \frac{1}{1+e^{-(w_1\times T_h+w_2\times T_c+w_3\times k_{alt}+w_4\times k_d+w_5\times k_p+\delta_j)}}$$

j	w_1	w_2	w_3	w_4	w_5	δ_j
Weights between input and first hidden layers for amplitude of displacer						
1	1.5438	−0.7490	−0.1218	−0.7454	−3.5411	−4.0067
2	−1.6502	1.7483	1.8423	2.1051	1.5649	2.4040
3	2.1550	2.2075	1.7635	1.8258	0.3055	−0.8013
4	2.1480	0.2705	−1.3701	2.2529	2.1009	0.8013
5	1.0449	3.1528	−0.7608	1.1137	1.7895	2.4040
6	1.8624	1.1396	2.5454	−2.0251	−2.0251	4.0067

Appendix F. . Weights among layers for amplitude of piston

$$M_i = \frac{1}{1+e^{-(w_1\times N_1+w_2\times N_2+w_3\times N_3+w_4\times N_4+w_5\times N_5+w_6\times N_6\ +\ \delta_i)}}$$

i	w_1	w_2	w_3	w_4	w_5	w_6	δ_i
Weights between first and second hidden layers for amplitude of piston							
1	0.7291	−0.8464	−0.7016	0.5645	0.635	0.3522	0.5143
2	−0.958	−0.2466	−0.9318	−0.3455	−0.6528	0.7512	−0.5407

$$N_j = \frac{1}{1+e^{-(w_1\times T_h+w_2\times T_c+w_3\times k_{alt}+w_4\times k_d+w_5\times k_p+\delta_j)}}$$

j	w_1	w_2	w_3	w_4	w_5	δ_j
Weights between input layer and first hidden layers for amplitude of piston						
1	1.9585	1.5657	−0.7622	2.2221	2.0611	−4.0067
2	−0.2531	−1.4154	−2.0507	−3.1032	−0.3887	2.404
3	2.2177	0.8945	−2.187	1.1476	2.058	−0.8013
4	−0.7518	0.677	−1.4131	2.6424	2.4162	−0.8013
5	0.8986	1.3648	−1.2664	3.1911	−1.2635	2.404
6	0.536	−1.6891	0.3178	−3.3844	1.1655	4.0067

Appendix G. . Weights among layers for operating frequency

$$M_i = \frac{1}{1+e^{-(w_1\times N_1+w_2\times N_2+w_3\times N_3+w_4\times N_4+w_5\times N_5+w_6\times N_6\ +\ \delta_i)}}$$

i	w_1	w_2	w_3	w_4	w_5	w_6	δ_i
Weights between first and second hidden layers for operating frequency							
1	−0.0033	−0.5524	0.3982	−0.7228	−0.4914	−0.3000	−0.0534
2	0.9195	0.5025	0.7818	−0.7014	0.6286	−0.6068	−0.2967
3	−0.3192	−0.4898	0.9186	−0.4850	−0.5130	−0.4978	0.6617
4	0.1705	0.0119	0.0944	0.6814	0.8585	0.2321	0.1705

$$N_j = \frac{1}{1+e^{-(w_1\times T_h+w_2\times T_c+w_3\times k_{alt}+w_4\times k_d+w_5\times k_p+\delta_j)}}$$

j	w_1	w_2	w_3	w_4	w_5	δ_j
Weights between input layer and first hidden layer for operating frequency						
1	1.5046	−2.7330	−1.0677	1.7233	1.4868	−4.0067
2	1.4367	−1.3181	2.6603	−1.8502	−1.3235	−2.4040
3	−0.6321	−2.6617	−2.7304	−0.0600	1.0539	0.8013
4	1.3365	−3.4632	−0.5266	−0.4678	1.3333	0.8013
5	−2.1897	2.1540	−0.7887	0.9743	−2.2468	−2.4040
6	1.4160	1.3389	1.8247	1.4388	−2.6184	4.0067

Appendix H. . Weights among layers for output power

$$M_i = \frac{1}{1 + e^{-(w_1 \times N_1 + w_2 \times N_2 + w_3 \times N_3 + w_4 \times N_4 + w_5 \times N_5 + w_6 \times N_6 + \delta_i)}}$$

i	w_1	w_2	w_3	w_4	w_5	w_6	δ_i
Weights between first and second hidden layers for output power							
1	−0.9552	−0.7183	−0.0684	−0.0111	0.7953	−0.4619	−0.0482
2	−0.8923	0.7869	0.1217	−0.8644	−0.4229	0.1884	−0.2634

$$N_j = \frac{1}{1 + e^{-(w_1 \times T_h + w_2 \times T_c + w_3 \times k_{alt} + w_4 \times k_d + w_5 \times k_p + \delta_j)}}$$

j	w_1	w_2	w_3	w_4	w_5	δ_j
Weights between input and first hidden layers for output power						
1	0.1282	−1.6680	−1.3136	−1.5505	3.0208	−4.0067
2	1.3379	1.4251	2.2888	−2.1067	1.5988	−2.4040
3	−0.7817	2.1146	−1.8503	2.0657	−1.8112	0.8013
4	−2.5763	0.1058	1.5102	1.3304	−2.3140	−0.8013
5	1.7996	2.5177	−0.4086	−0.4456	2.4720	2.4040
6	−2.1019	−1.6170	1.8408	−2.3733	−0.0189	−4.0067

References

[1] G. Walker, J.R. Senft, Free Piston Stirling Engines, Springer-Verlag, Berlin, 1985.
[2] D. Shrestha, Numerical and experimental studies on free piston Stirling engines (Master of Science dissertation), University of Maryland, Maryland, USA, 2012.
[3] A.R. Tavakolpour Saleh, S.H. Zare, H. Bahreman, A novel active free piston Stirling engine: modeling, development, and experiment, Appl. Energy 199 (2017) 400–415.
[4] A. Abuelyamen, R.B. Mansour, H. Abualhamayel, et al., Parametric study on beta-type Stirling engine, Energy Convers. Manage. 145 (2017) 53–63.
[5] S.H. Zare, A.R. Tavakolpour Saleh, Free piston Stirling engines: A review, Int. J. Energy Res. 44 (2020) 5039–5070.
[6] J.G.M. Saturno, Some mathematical model to describe the dynamic behavior of the B10 free-piston Stirling engine, PhD thesis, Ohio University, London, 1994.
[7] Y.C. Hsieh, T.C. Hsu, J.S. Chiou, Integration of a free-piston Stirling engine and a moving grate incinerator, Renew. Energy 33 (2008) 48–54.
[8] E.D. Rogdakis, N.A. Bormpilas, I.K. Koniakos, A thermodynamic study for the optimization of stable operation of free piston Stirling engines, Energy Convers. Manage. 45 (2004) 575–593.
[9] H. Karabulut, Dynamic analysis of a free piston Stirling engine working with closed and open thermodynamic cycles, Renew. Energy 36 (2011) 1704–1709.
[10] S. Kwankaomeng, B. Silpsakoolsook, P. Savangvong, Investigation on Stability and Performance of a Free-Piston Stirling Engine, Energy Procedia 52 (2014) 598–609.
[11] N.A. Khripach, D.A. Ivanov, L.Y. Lezhnev, Calculation studies of a free-piston Stirling engine, J. Ind. Pollut. Control 33 (2) (2017) 1603–1611.
[12] K. Sim, D.J. Kim, Identification of Damping Characteristics of Free-piston Stirling Engines via Nonlinear Dynamic Model Predictions, Trans. Korean Soc. Noise Vib. Eng. 26 (3) (2016) 248–257.
[13] K. Sim, D.J. Kim, Dynamic model prediction and validation for free-piston Stirling engines considering nonlinear load damping, Trans. Korean Soc. Mech. Eng. 39 (10) (2015) 985–993.
[14] N. Ulusoy, Dynamic analysis of free piston Stirling engines, Case Western Reserve University (1994).
[15] A.R. Tavakolpour-Saleh, S. Zare, A. Omidvar, Applying perturbation technique to analysis of a free piston Stirling engine possessing nonlinear springs, Appl. Energy 183 (2016) 526–541.
[16] S. Zare, A.R. Tavakolpour-Saleh, A.R. Shourangiz-Haghighi, et al., Assessment of damping coefficients ranges in design of a free piston Stirling engine: Simulation and experiment, Energy 185 (2019) 633–643.
[17] F. Cascella, M. Sorin, F. Forsosa, et al., Modeling the dynamic and thermodynamic operating of Stirling engines by means of an equivalent electrical circuit, Energy Convers. Manage. 150 (2017) 295–303.
[18] M. Majidniya, T. Boileau, B. Remy, et al., Nonlinear modeling of a Free Piston Stirling Engine combined with a Permanent Magnet Linear Synchronous Machine, Appl. Therm. Eng. 165 (2020), 114544.
[19] L.K. Tartibu, B. Sun, A.E. Kaunda, Multi-objective optimization of the stack of a thermoacoustic engine using GAMS, Appl. Software Comput. 28 (2015) 30–43.
[20] G.Y. Zhong, P. Yang, Y.W. Liu, Heat transfer and pressure drop correlations by means of response surface methodology, Int. J. Heat Mass Transf. 119 (2018) 312–332.
[21] P. Yang, Y.W. Liu, Prediction and parametric analysis of acoustic streaming in a thermoacoustic Stirling heat engine with a jet pump using response surface methodology, Appl. Therm. Eng. 103 (2016) 1004–1013.
[22] C.L. Diel, R.L. Canevesi, D.A. Zempulski, et al., Optimization of multiple-effect evaporation in the pulp and paper industry using response surface methodology, Appl. Therm. Eng. 95 (2016) 18–23.
[23] W.L. Ye, P. Yang, Y.W. Liu, Multi-objective thermodynamic optimization of a free piston Stirling engine using response surface methodology, Energy Convers. Manage. 176 (2018) 147–163.
[24] H. Solmaz, S.M.S. Ardebili, F. Aksoy, et al., Optimization of the operating conditions of a beta-type rhombic drive Stirling engine by using response surface method, Energy 198 (2020), 117377.
[25] B. Ghobadian, H. Rahimi, A.M. Nikbakht, et al., Diesel engine performance and exhaust emission analysis using waste cooking biodiesel fuel with an artificial neural network, Renew. Energy 34 (2009) 976–982.
[26] M.H. Ahmadi, Prediction of power in solar Stirling heat engine by using neural network based on hybrid genetic algorithm and particle swarm optimization, Neural Comput. Appl. 22 (2013) 1141–1150.
[27] Yasar Önder Özgören, Selim Çetinkaya, Artificial neural network-based modelling of performance of a beta-type Stirling engine, Proc. Inst. Mech. Eng. 227 (3) (2012) 166–177.
[28] W.L. Ye, X.J. Wang, Y.W. Liu, Application of artificial neural network for predicting the dynamic performance of a free piston Stirling engine, Energy 194 (2020), 116912.
[29] W.L. Ye, T. Zhang, X.J. Wang, et al., Parametric study of gamma-type free piston Stirling engine using nonlinear thermodynamic-dynamic coupled model, Energy 211 (2020), 118458.
[30] I. Korkut, A. Acir, M. Boy, Application of regression and artificial neural network analysis in modeling of tool-chip interface temperature in machining, Expert Syst. Appl. 38 (2011) 11651–11656.
[31] Z. Zhang, K. Friedrich, Artificial neural networks applied to polymer composites: a review, Compos. Sci. Technol. 63 (2003) 2029–2044.
[32] M. Hooshang, R.A. Moghadam, S.A. Nia, et al., Optimization of Stirling engine design parameters using neural networks, Renew. Energy 74 (2015) 855–866.
[33] A.A. Rahman, X.Q. Zhang, Prediction of oscillatory heat transfer coefficient for a thermoacoustic heat exchanger through artificial neural network technique, Int. J. Heat Mass Transf. 124 (2018) 1088–1096.
[34] A. Parlak, Y. Islamoglu, H. Yasar, et al., Application of artificial neural network to predict specific fuel consumption and exhaust temperature for a Diesel engine, Appl. Therm. Eng. 26 (2006) 824–828.
[35] Ç. Yusuf, Ç. Adem, K. Fuat, et al., Prediction of engine performance for an alternative fuel using artificial neural network, Appl. Therm. Eng. 37 (2012) 217–225.
[36] R.K. Mehra, H. Duan, S.J. Luo, A. Rao, F.H. Ma, Experimental and artificial neural network study of hydrogen enriched compressed natural gas engine under various ignition timings and excess air ratios, Appl. Energy 228 (2018) 736–754.
[37] S.M. Miraboutalebi, P. Kazemi, P. Bahrami, Fatty Acid Methyl Ester composition used for estimation of biodiesel cetane number employing random forest and artificial neural networks: A new approach, Fuel 166 (2016) 143–151.